RSC Advances

PAPER

View Article Online
View Journal | View Issue

Check for updates

Cite this: *RSC Adv.*, 2019, **9**, 30406

# A single-phase white light emitting phosphor $Ba_3Y(PO_4)_3:Ce^{3+}/Tb^{3+}/Mn^{2+}$: luminescence, energy transfer and thermal stability

Yun Chen, Wenge Ding,* Panlai Li,* Xue Li, Qi Bao, Jinjin Liu, Keliang Qiu, Xiangyu Meng, Zhiping Yang and Zhijun Wang*

Received 2nd August 2019
Accepted 16th September 2019

DOI: 10.1039/c9ra05995d

rsc.li/rsc-advances

A series of $Ce^{3+}/Tb^{3+}$, $Tb^{3+}/Mn^{2+}$ and $Ce^{3+}/Tb^{3+}/Mn^{2+}$ doped $Ba_3Y(PO_4)_3$ were synthesized by the high temperature solid state method. Phase formation, energy transfer, luminescence properties and thermal quenching properties of phosphors were analyzed in detail. For the co-doped samples, the energy transfer from $Ce^{3+}$ to $Tb^{3+}$ and $Tb^{3+}$ to $Mn^{2+}$ was proved by analyzing the spectra and fluorescence lifetime, and the energy transfer mechanism was calculated to be dipole–dipole interaction. A series of color-tunable phosphors were obtained by the energy transfer from $Ce^{3+}$ to $Tb^{3+}$ and $Tb^{3+}$ to $Mn^{2+}$. For the tri-doped samples, it was confirmed that the energy transfers from $Ce^{3+}$ to $Tb^{3+}$, $Tb^{3+}$ to $Mn^{2+}$ and $Ce^{3+}$ to $Mn^{2+}$ exist at the same time by analyzing the spectra properties, and it can emit warm-white light with extensive color temperature regulability. In addition, the thermal stability was abnormal and outstanding because the defects exist in the samples. The results show that the phosphors may be novel warm white emitting phosphors for white light emitting diodes.

Open Access Article. Published on 25 September 2019. Downloaded on 6/30/2024 12:57:32 PM.
This article is licensed under a Creative Commons Attribution-NonCommercial 3.0 Unported Licence.

## 1 Introduction

In recent years, white-light-emitting diodes (LEDs) have received more and more attention for their many advantages[1] Compared with traditional light sources, white LEDs have higher efficiency, higher brightness, longer service time and are more environmentally friendly, hence they are considered as the fourth generation light source.[1–7] The most common method to synthesize white LEDs is to combine the GaN blue LED chip with yellow phosphor YAG:$Ce^{3+}$. However, this type of white LED has many drawbacks due to lack of a red ingredient, such as the poor color rendering index and the high correlated color temperature.[3,4,8] Because white LEDs can not only be used in lighting field, but also in display and medical fields, hence they should show specific optical performance in different application scenarios which means that phosphors with high tunability are needed.[7,9] Nowadays, the ultraviolet-excited single-phased phosphors have been taken seriously, which can achieve white light with good color rendering index, suitable correlated color temperature and tunable emission by adjusting the doping ratio of different ions.[10–13] Therefore, it is urgent to find novel and high performance single-phased phosphors. Generally, when doping rare earth ions or transition metal ions into compound, the white emitting phosphor may be achieved by the energy transfer between different activator ions,[14] such as $Ca_{10}Na(PO_4)_7:Ce^{3+}/Tb^{3+}/Mn^{2+}$,[15] $Na_2Ba_6(Si_2O_7)(SiO_4)_2:Ce^{3+}/Eu^{2+}/Tb^{3+}/Mn^{2+}$.[16] Among many host compounds, the eulytite-type orthophosphates with the type of $M_3^{I}M^{II}(PO_4)_3$ ($M^{I}$ = Ba, Sr, Ca, and Pb, $M^{II}$ = La, Sc, Y, Bi, and In) have attracted great interests, for example, when doped $Ce^{3+}$, $Tb^{3+}$, and $Mn^{2+}$ in $Ba_3Y(PO_4)_3$ (BYP), the phosphors can produce blue, green and red light, respectively.[17–19] Thus, it is possible to achieve white emission when the above three ions are tri-doped in BYP. Moreover, the thermal stability of phosphor is an essential characteristic. It has been reported in our previous work that BYP:$Ce^{3+}$,$Mn^{2+}$ shows extraordinary thermal stability due to the existence of defect in the samples.[17] It is expectable that the defect is to be utilized to gain a series of phosphors with high temperature stability in $Ce^{3+}/Tb^{3+}/Mn^{2+}$ doped BYP. In this work, series of $Ce^{3+}/Tb^{3+}$, $Tb^{3+}/Mn^{2+}$ or $Ce^{3+}/Tb^{3+}/Mn^{2+}$ doped BYP are obtained. Phase formation, energy transfer, luminescence properties and thermal property were investigated in detail. Finally, series of single-phased white emitting phosphors are obtained by the energy transfer $Ce^{3+} \rightarrow Tb^{3+}$, $Tb^{3+} \rightarrow Mn^{2+}$ and $Ce^{3+} \rightarrow Mn^{2+}$.

## 2 Experimental

### 2.1 Sample preparation

Series of $Ba_3Y_{0.95-x}(PO_4)_3:0.05Ce^{3+},xTb^{3+}$, $Ba_{3-y}Y_{0.95}(PO_4)_3:0.05Ce^{3+},yMn^{2+}$ and $Ba_{2.86}Y_{0.7-z}(PO_4)_3:zCe^{3+},0.3Tb^{3+},0.14Mn^{2+}$ were synthesized by a high temperature solid state method. Raw materials $BaCO_3$

*National-Local Joint Engineering Laboratory of New Energy Photoelectric Devices, Hebei Key Laboratory of Optic-electronic Information and Materials, College of Physics Science & Technology, Hebei University, Baoding 071002, China. E-mail: dwg@hbu.edu.cn; li_panlai@126.com; wangzj1998@126.com*



This journal is © The Royal Society of Chemistry 2019

Open Access Article. Published on 25 September 2019. Downloaded on 6/30/2024 12:57:32 PM.
This article is licensed under a Creative Commons Attribution-NonCommercial 3.0 Unported Licence.

(analytical reagents, A.R.), $NH_4H_2(PO_4)_3$ (A.R.), $Y_2O_3$ (99.99%), $CeO_2$ (99.99%), $Tb_4O_7$ (99.99%) and $MnCO_3$ (A.R.) were weighed according to stoichiometric proportions, and then mixed them in an agate mortar pestling for 20 min to ensure the materials are distributed uniformly. The mixed materials were put into crucibles and heated at 1300 °C for 3 h in a carbon reducing atmosphere. After firing, the samples cooled to room temperature slowly and were grounded into powder for subsequent use.

### 2.2 Materials characterization

XRD patterns of sample are measured by powder X-ray diffraction (XRD) using a D8-A25 Focus diffractometer at 40 kV and 40 mA with step size of 0.05° and a scan speed 0.1 s per step. Spectral property of sample was measured by Hitachi F-4600 fluorescence spectrophotometer with a 450 W Xe lamp as the excitation source. Decay curves were measured by Horiba FL-4600 fluorescence spectrophotometer with a 320 nm pulse laser radiation (nano-LED) for $Ce^{3+}$ and 450 W Xe lamp as the excitation resource for $Mn^{2+}$ at room temperature. Thermoluminescence spectra of samples were measured by a FJ-427A1 TL dosimeter at room temperature with a fixed heating rate of 1 k $s^{-1}$ within the range 300–450 K. Commission Internationale de L'Eclairage (CIE) chromaticity coordinates of samples were obtained by the PMS-80 spectral analysis system.

## 3 Results and discussion

### 3.1 Phase formation

The XRD patterns of BYP:0.05$Ce^{3+}$,$x$$Tb^{3+}$ ($x$ = 0.02, 0.45), BYP:0.05$Ce^{3+}$,$y$$Mn^{2+}$ ($y$ = 0.08, 0.14) and BYP:$z$$Ce^{3+}$,0.3$Tb^{3+}$,0.14$Mn^{2+}$ ($z$ = 0.07, 0.15) were shown in Fig. 1. It can be seen that no apparent impurity phase appears and all the diffraction peaks of samples can be indexed to the standard card of BYP (JCPDS No. 44-0318) appropriately. The XRD patterns illustrates that $Ce^{3+}$, $Tb^{3+}$ and $Mn^{2+}$ did not cause any significant change to the crystal structure of BYP and series of pure phase phosphors were obtained.

### 3.2 Luminescence and energy transfer properties of BYP:$Ce^{3+}$,$x$$Tb^{3+}$

Fig. 2a–c display the emission and excitation spectra of BYP:0.05$Ce^{3+}$ ($\lambda_{ex}$ = 330 nm, $\lambda_{em}$ = 400 nm), BYP:0.45$Tb^{3+}$ ($\lambda_{ex}$ = 377 nm, $\lambda_{em}$ = 550 nm) and BYP:0.05$Ce^{3+}$,0.15$Tb^{3+}$ ($\lambda_{ex}$ = 330 nm, $\lambda_{em}$ = 400 nm, 550 nm), respectively. The emission spectrum of BYP:0.05$Ce^{3+}$ shows a blue emission band peaking at 400 nm, which originates from the electron transition 5d → 4f of $Ce^{3+}$. The excitation band of BYP:0.05$Ce^{3+}$ ranges from 200 nm to 360 nm ($\lambda_{max}$ = 330 nm) due to the 4f → 5d electron transition. For BYP:0.45$Tb^{3+}$, a series of characteristic emission peaks of $Tb^{3+}$ appear in the emission spectrum which originates from the electron transition $^5D_4 \rightarrow {}^7F_6$ (500 nm), $^5D_4 \rightarrow {}^7F_5$ (550 nm), $^5D_4 \rightarrow {}^7F_4$ (590 nm) and $^5D_4 \rightarrow {}^7F_3$ (630 nm) of $Tb^{3+}$, respectively. The excitation spectrum of BYP:0.45$Tb^{3+}$ shows a broad excitation band from 210 nm to 400 nm because of the allowed $4f^8$–$4f^7$5d transition and intra-configuration transition of $Tb^{3+}$. Comparing the emission spectrum of BYP:0.05$Ce^{3+}$ with the excitation spectrum of BYP:0.45$Tb^{3+}$, an obvious spectral overlapping can be observed which means an effective energy transfer from $Ce^{3+}$ to $Tb^{3+}$ ($ET_{Ce-Tb}$) may be occur.[19,20] In addition, the emission spectrum of BYP:0.05$Ce^{3+}$,0.15$Tb^{3+}$ contains both the emission band of $Ce^{3+}$ and $Tb^{3+}$, the excitation spectrum monitored at 550 nm (emission peak of $Tb^{3+}$) has the similar profile with that monitored at 400 nm (emission peak of $Ce^{3+}$), it also means that there may be energy transfer from $Ce^{3+}$ to $Tb^{3+}$.

In order to further investigate the luminescence properties, a series of BYP:$Ce^{3+}$,$x$$Tb^{3+}$ were synthesized. Fig. 3a shows the emission spectra of BYP:0.05$Ce^{3+}$,$x$$Tb^{3+}$ ($x$ = 0–0.45) under 330 nm UV excitation. Fig. 3b reveals the emission intensity of $Ce^{3+}$ ($\lambda_{em}$ = 400 nm) and $Tb^{3+}$ ($\lambda_{em}$ = 550 nm), it can be seen that the emission intensity of $Ce^{3+}$ declines constantly as the concentration of $Tb^{3+}$ increasing, meanwhile, the emission intensity of $Tb^{3+}$ goes up ceaselessly. According to the change of emission intensity, it means that an effective energy transfer from $Ce^{3+}$ to $Tb^{3+}$ is expectable.

To confirm the energy transfer from $Ce^{3+}$ to $Tb^{3+}$, the decay curves of $Ce^{3+}$ monitored at 400 nm under 320 nm pulse laser radiation (nano-LED) excitation and decay curves of $Tb^{3+}$ monitored at 550 nm under 377 nm excitation for BYP:0.05$Ce^{3+}$,$x$$Tb^{3+}$ are shown in Fig. 4a and b, respectively. The decay curves of $Ce^{3+}$ and $Eu^{2+}$ can be matched well with second-order exponential function, which can be expressed as the following expression:[21,22]

$$I_{(t)} = A_1 \exp(t/\tau_1) + A_2 \exp(t/\tau_2) \quad (1)$$

where $I_{(t)}$ is the luminescence intensity, $A_1$ and $A_2$ are constants, $t$ is time, $\tau_1$ and $\tau_2$ are the lifetimes for the exponential components. The average lifetime $\tau^*$ can be calculated by the following formula[21,23]

$$\tau^* = (A_1\tau_1^2 + A_2\tau_2^2)/(A_1\tau_1 + A_2\tau_2) \quad (2)$$

The calculated average lifetime of $Ce^{3+}$ and $Tb^{3+}$ are shown in Fig. 4c, from which one can see that the lifetime of $Ce^{3+}$ decreases consistently and that of $Tb^{3+}$ increases consistently with increasing $Tb^{3+}$ concentration. The lifetime can strongly prove the energy transfer from $Ce^{3+}$ to $Tb^{3+}$, and the energy transfer efficiency can be calculated by the following equation[9,22]

$$\eta_T = 1 - \tau/\tau_0 \quad (3)$$

where $\tau$ and $\tau_0$ are the decay time of the sensitizer $Ce^{3+}$ in the presence and absence of activator $Tb^{3+}$, respectively. Fig. 4d shows that the energy transfer efficiency rises up constantly with increase $Tb^{3+}$ concentration, and the maximum value is 69.9% when the doping concentration of $Tb^{3+}$ reaches the maximum $x$ = 0.45.

According to Dexter's theory, there are two types of interactions between sensitizers and activators: multipolar interaction and exchange interaction.[21,24] The critical distance between $Ce^{3+}$ and $Tb^{3+}$ ($R_{Ce-Tb}$) is a critical factor to judge which type it

Open Access Article. Published on 25 September 2019. Downloaded on 6/30/2024 12:57:32 PM.
This article is licensed under a Creative Commons Attribution-NonCommercial 3.0 Unported Licence.

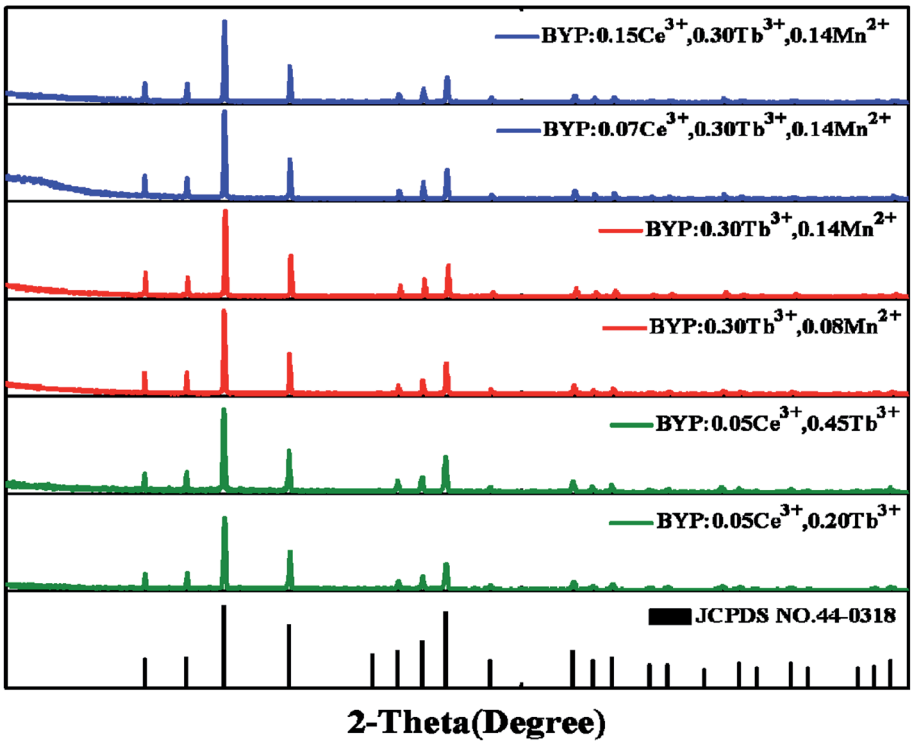


Fig. 1 XRD patterns of the representative samples and the standard patterns of $Ba_3Y(PO_4)_3$ (JCPDS No. 44-0318).

belongs to, and the critical distance $R_{Ce-Tb}$ can be calculated by the following formula[25]

$$R_c = 2\left[\frac{3V}{4N\pi\chi_c}\right]^{\frac{1}{3}} \quad (4)$$

where $N$ is the number of the cations in host, $V$ is the volume of the unit cell. $\chi_c$ is the sum of $Ce^{3+}$ and $Tb^{3+}$ concentration when the emission intensity of $Ce^{3+}$ in the presence of $Tb^{3+}$ is half that in the absence of $Tb^{3+}$. Herein, $V$ equals to 1165.61 $Å^3$ and $N$ equals to 4, $\chi_c$ is calculated to be 0.2. Thus, the $R_{Ce-Tb}$ is calculated to be 17.72 Å which is larger than the maximum distance of 5 Å for the exchange interaction, it means the energy

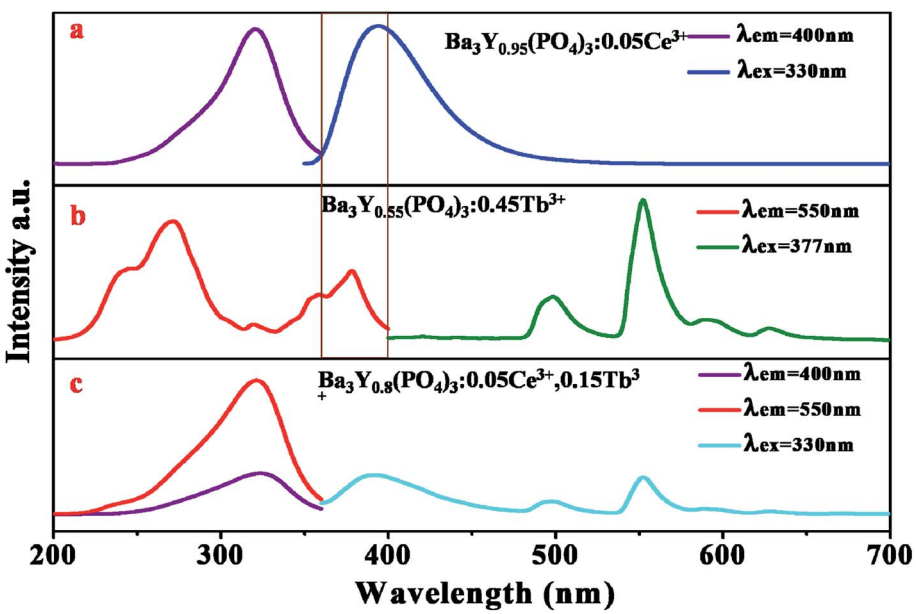


Fig. 2 Emission and excitation spectra of (a) BYP:0.05$Ce^{3+}$; (b) BYP:0.45$Tb^{3+}$; (c) BYP:0.05$Ce^{3+}$,0.15$Tb^{3+}$.

 This journal is © The Royal Society of Chemistry 2019

Open Access Article. Published on 25 September 2019. Downloaded on 6/30/2024 12:57:32 PM.
This article is licensed under a Creative Commons Attribution-NonCommercial 3.0 Unported Licence.

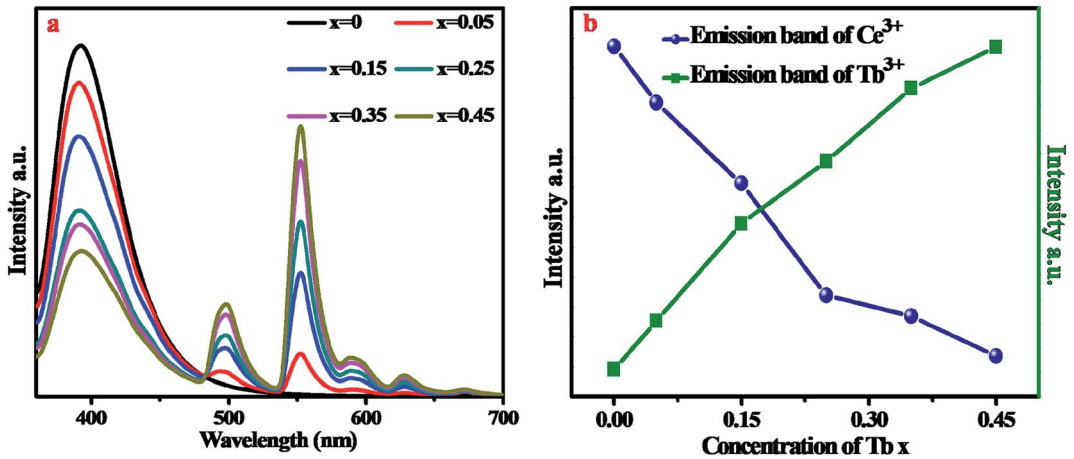


Fig. 3 (a) Emission spectra of BYP:0.05$Ce^{3+}$,x$Tb^{3+}$ ($x = 0$–0.45). (b) Emission intensity of $Ce^{3+}$ and $Tb^{3+}$ as a function of $Tb^{3+}$ concentration.

transfer mechanism of $Ce^{3+}$–$Tb^{3+}$ belongs to multipolar interaction.

There are three kinds of multipolar interactions: dipole–dipole, dipole–quadrupole and quadrupole–quadrupole interaction. The mechanism of $ET_{Ce-Tb}$ can be discussed by Dexter's theory:[24,26]

$$\frac{I_{s0}}{I_s} \propto C^{\frac{n}{3}} \quad (5)$$

where $I_{s0}$ and $I_s$ are the emission intensity of sensitizer $Ce^{3+}$ in the absence and presence of the activator $Tb^{3+}$, respectively. The sum concentration of $Ce^{3+}$ and $Tb^{3+}$ is represented by $C$. Herein, $n = 6$, 8 and 10 correspond to dipole–dipole, dipole–quadrupole

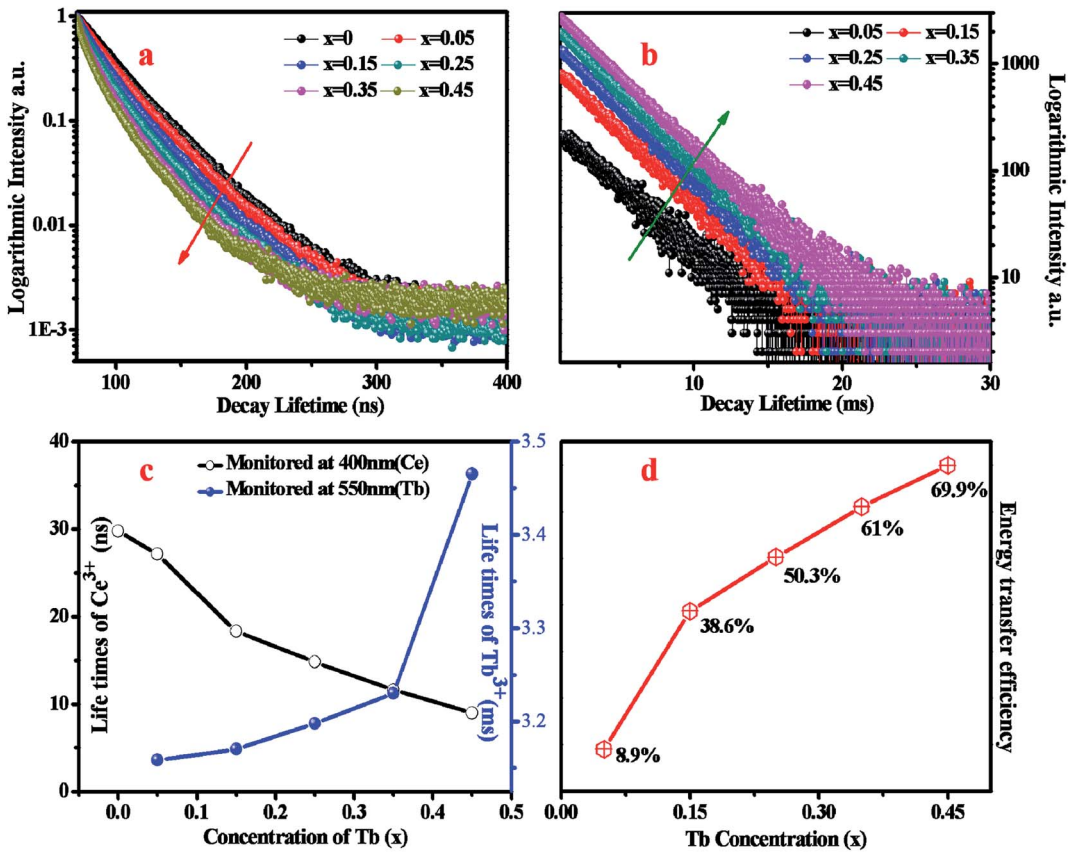


Fig. 4 (a) Decay curves of $Ce^{3+}$ in BYP:0.05$Ce^{3+}$,x$Tb^{3+}$ ($\lambda_{em} = 400$ nm, $\lambda_{ex} = 320$ nm). (b) Decay curves of $Tb^{3+}$ in BYP:0.05$Ce^{3+}$,x$Tb^{3+}$ ($\lambda_{em} = 550$ nm, $\lambda_{ex} = 377$ nm). (c) Lifetime of $Ce^{3+}$ and $Tb^{3+}$ as function of $Tb^{3+}$ concentration. (d) Energy transfer efficiency from $Ce^{3+}$ to $Tb^{3+}$ as function of $Tb^{3+}$ concentration.

Open Access Article. Published on 25 September 2019. Downloaded on 6/30/2024 12:57:32 PM.
This article is licensed under a Creative Commons Attribution-NonCommercial 3.0 Unported Licence.

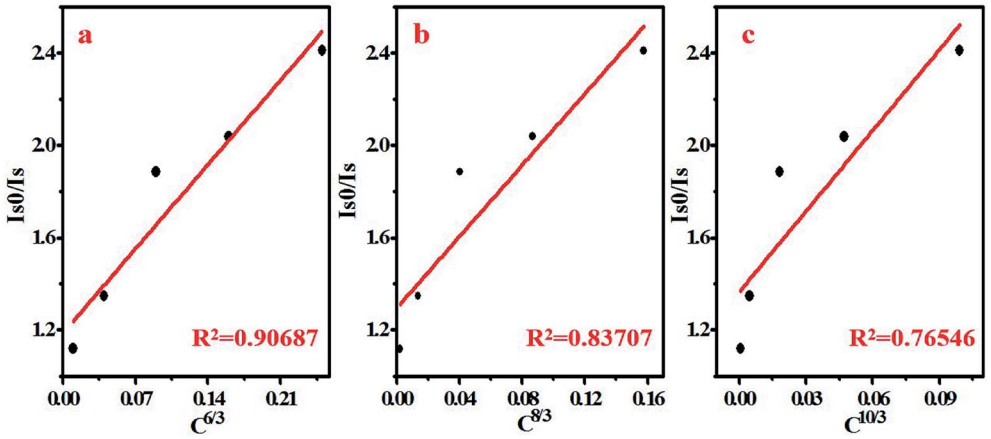


Fig. 5 Dependence of $I_{s0}/I_s$ of $Ce^{3+}$ and $Tb^{3+}$ on $C^{6/3}$, $C^{8/3}$ and $C^{10/3}$ in BYP:0.05$Ce^{3+}$,x$Tb^{3+}$.

and quadrupole–quadrupole interactions, respectively.[24,26,27] The linear relationship between $I_{s0}/I_s$ and $C^{n/3}$ for BYP:0.05$Ce^{3+}$,x$Tb^{3+}$ are illustrated in Fig. 5, it can be seen that a well fitted curve can be gotten when $n = 6$ ($R^2 = 0.94952$), hence it can be concluded that the dipole–dipole interaction plays an essential role in the energy transfer from $Ce^{3+}$ to $Tb^{3+}$.

The Commission Internationale de L'Eclairage (CIE) chromaticity coordinates of BYP:0.05$Ce^{3+}$,x$Tb^{3+}$ ($x$ = 0–0.45) was calculated basing on the relevant emission spectra under 330 nm excitation. The results along with luminescent photographs of related phosphors are depicted in Fig. 6, the emission color of BYP:0.05$Ce^{3+}$,x$Tb^{3+}$ can be modulated from blue (0.1622, 0.0406) to yellow-green (0.2946, 0.4169). Hence, series of color-tunable phosphors were synthesized successfully.

To analyze the thermal stability of BYP:0.05$Ce^{3+}$,x$Tb^{3+}$, the temperature-dependent emission spectra of BYP:0.05$Ce^{3+}$,0.45$Tb^{3+}$ excited by 330 nm were measured which is shown in Fig. 7a, and the emission intensity of $Ce^{3+}$ and $Tb^{3+}$ with increasing the temperature is depicted in Fig. 7b. It can be seen from the pictures that the emission intensity of $Ce^{3+}$ shows a first increases and then decreases with increasing the temperature, but it remains 107.7% of the initial value (300 K) when the temperature reaches 425 K. As for $Tb^{3+}$, its emission intensity increases constantly and reaches to 138.8% of the initial value when the temperature reaches 425 K. The abnormal change of emission intensity of $Ce^{3+}$ and $Tb^{3+}$ with temperature may be caused by the defects in BYP:0.05$Ce^{3+}$,0.45$Tb^{3+}$.[28–30] Fig. 8a shows the thermoluminescence spectrum of BYP:0.05$Ce^{3+}$,0.45$Tb^{3+}$, it can be seen that there are two emission bands ranging from 400 K to 420 K and from 460 K to 480 K, respectively. The thermoluminescence spectrum confirms the existence of defects. Fig. 8b depicts how defects affect the thermal stability of BYP:0.05$Ce^{3+}$,x$Tb^{3+}$: the shallow trap D1 and deep trap D2 can store the electrons, but the electrons transmit to the conduction band when BYP:0.05$Ce^{3+}$,x$Tb^{3+}$ are heated. After that, a part of electrons transmit to $^5D_4$ energy level of $Tb^{3+}$ and 5d energy band of $Ce^{3+}$ from conduction band, then more

| CIE chromaticity coordinates ofBYP:0.05$Ce^{3+}$,x$Tb^{3+}$ | |
|---|---|
| x=0 | (0.1622 , 0.0406) |
| x=0.05 | (0.1909 , 0.1225) |
| x=0.15 | (0.2352 , 0.2486) |
| x=0.25 | (0.2677 , 0.3380) |
| x=0.35 | (0.2838 , 0.3876) |
| x=0.45 | (0.2946 , 0.4169) |

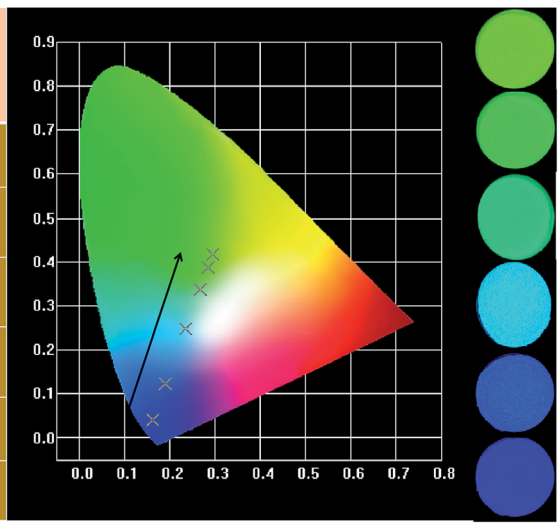

Fig. 6 CIE chromaticity coordinates of BYP:0.05$Ce^{3+}$,x$Tb^{3+}$ ($x$ = 0–0.45) along with their luminescent photographs.


This journal is © The Royal Society of Chemistry 2019

Open Access Article. Published on 25 September 2019. Downloaded on 6/30/2024 12:57:32 PM.
This article is licensed under a Creative Commons Attribution-NonCommercial 3.0 Unported Licence.

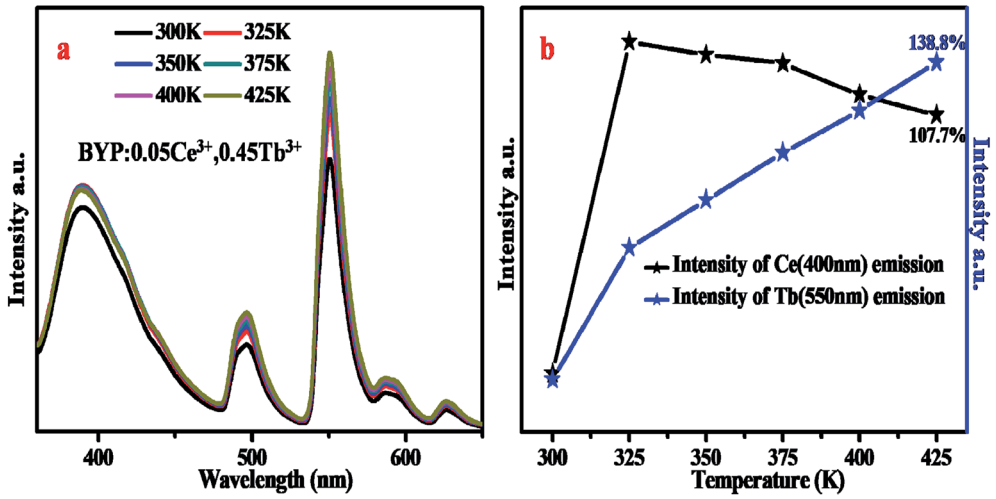


Fig. 7 (a) Temperature-dependent emission spectra of BYP:0.05$Ce^{3+}$,x$Tb^{3+}$ excited by 330 nm. (b) Relative intensity of $Ce^{3+}$ and $Tb^{3+}$ in the temperature-dependent emission spectra.

electrons transmit from $^5D_4$ to $^7F_J$ energy level and 5d to 4f energy band by radiative transition meaning more energy would be released. Thus, the emission intensity of $Ce^{3+}$ and $Tb^{3+}$ rise up with increasing temperature.[29]

### 3.3 Luminescence and energy transfer of BYP:0.4$Tb^{3+}$,y$Mn^{2+}$

The emission spectra of BYP:0.4$Tb^{3+}$,y$Mn^{2+}$ excited by 377 nm UV-light are shown in Fig. 9a and the relative emission intensities at 550 nm and 600 nm are depicted in Fig. 9b. The emission intensity of $Tb^{3+}$ (550 nm) decreases constantly with increasing $Mn^{2+}$ concentration, it means that $Mn^{2+}$ may absorb energy from $Tb^{3+}$. It is worth noting that the emission peaks of $Tb^{3+}$ and $Mn^{2+}$ coexist at 600 nm, as increasing $Mn^{2+}$ concentration the source of the peak at 600 nm change from $Tb^{3+}$ ($^5D_4$–$^7F_4$) to both $Mn^{2+}$ ($^4T_1$–$^6A_1$) and $Tb^{3+}$ and $Mn^{2+}$ is a main source. The intensity of the peak at 600 nm shows a first decrease, then increase and decrease in the end. The possible energy transfer maybe the main reason for the intensity changing: as increasing $Mn^{2+}$ concentration the energy transfer from $Tb^{3+}$ to $Mn^{2+}$ started to work, thus the emission intensity shows a first decrease; after that, the concentration of $Mn^{2+}$ is enough, hence the source of the emission peak mainly originates from $Mn^{2+}$ and the emission intensity of $Tb^{3+}$ is too low, thus the emission intensity of the peak at 600 nm started to pick up. In the end, the concentration of $Mn^{2+}$ reaches the quenching point, so its emission intensity started to decrease again.

To confirm the energy transfer from $Tb^{3+}$ to $Mn^{2+}$ in BYP:0.4$Tb^{3+}$,y$Mn^{2+}$, the decay curves of $Tb^{3+}$ ($\lambda_{em}$ = 550 nm, $\lambda_{ex}$ = 377 nm) and monitored at 600 nm (including $Tb^{3+}$ and $Mn^{2+}$, $\lambda_{ex}$ = 377 nm) are shown in Fig. 10a and b, respectively. The decay curves can be matched well with second-order exponential function expression (2), by means of expression (2) the

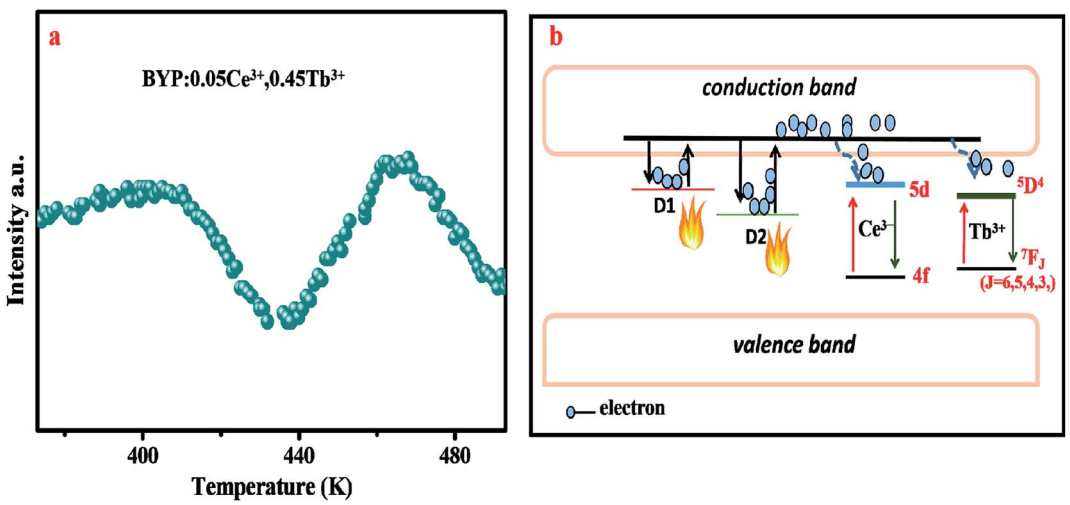


Fig. 8 (a) Thermoluminescence spectrum of BYP:0.05$Ce^{3+}$,0.45$Tb^{3+}$. (b) Schematic diagram of the interaction between the defect and temperature-dependent emission intensity in BYP:0.05$Ce^{3+}$,0.45$Tb^{3+}$.

Open Access Article. Published on 25 September 2019. Downloaded on 6/30/2024 12:57:32 PM.
This article is licensed under a Creative Commons Attribution-NonCommercial 3.0 Unported Licence.

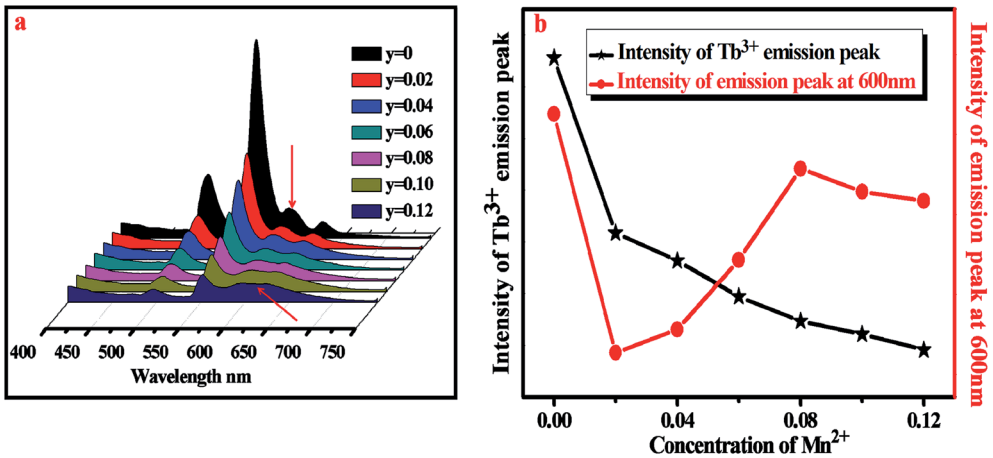


Fig. 9 (a) Emission spectra of BYP:0.4$Tb^{3+}$,y$Mn^{2+}$ ($y = 0$–0.12). (b) Relative emission intensity at 550 nm and 600 nm.

average lifetimes can be calculated and the results are shown in Fig. 10c. It can be seen that the lifetime of $Tb^{3+}$ decreases constantly as increasing $Mn^{2+}$ concentration, this can prove the energy transfer from $Tb^{3+}$ to $Mn^{2+}$ ($ET_{Ce-Tb}$). In addition, the lifetime monitored at 600 nm shows a first decrease when $y = 0$ rises to $y = 0.02$, then increase when $y = 0.02$ rises to $y = 0.08$. This phenomenon is due to the low concentration of $Mn^{2+}$ at the beginning, the measured and calculated lifetimes are mainly originated from $Tb^{3+}$, hence the lifetime decrease. When increased $Mn^{2+}$ concentration, it passed into the lifetime of $Mn^{2+}$, thus the lifetime starts to increase.

The energy transfer efficiency of $ET_{Tb-Mn}$ had been calculated by formula (3) and the results are shown in Fig. 10d. It can be seen that the energy transfer efficiency increases as $Mn^{2+}$ concentration increasing and the maximum value is 52.3% when $y = 0.12$. The critical distance from $Tb^{3+}$ to $Mn^{2+}$ ($Rc_{Tb-Mn}$)

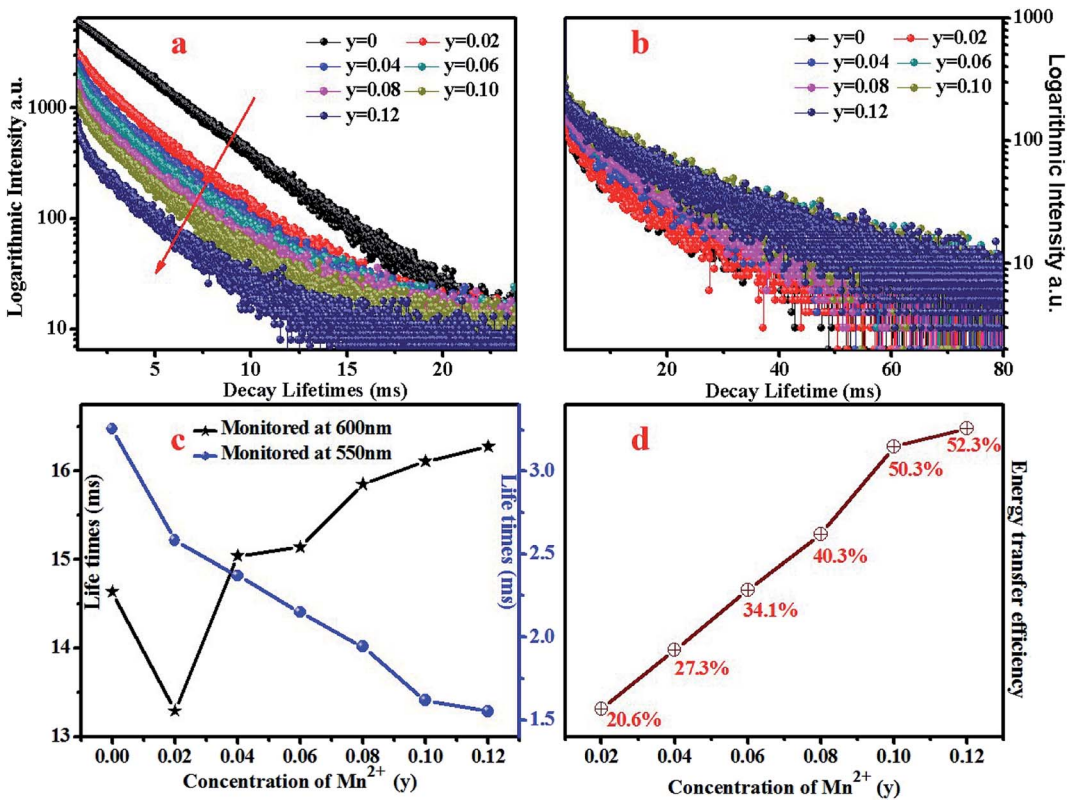


Fig. 10 (a) Decay curves of $Tb^{3+}$ in BYP:0.4$Tb^{3+}$,y$Mn^{2+}$ ($\lambda_{em} = 550$ nm, $\lambda_{ex} = 377$ nm). (b) Decay curves of $Tb^{3+}$ and $Mn^{2+}$ in BYP:0.4$Tb^{3+}$,y$Mn^{2+}$ ($\lambda_{em} = 600$ nm, $\lambda_{ex} = 377$ nm). (c) Lifetime of $Tb^{3+}$ and $Mn^{2+}$ as function of $Mn^{2+}$ concentration. (d) Energy transfer efficiency from $Tb^{3+}$ to $Mn^{2+}$ as function of $Mn^{2+}$ concentration.


This journal is © The Royal Society of Chemistry 2019

Open Access Article. Published on 25 September 2019. Downloaded on 6/30/2024 12:57:32 PM.
This article is licensed under a Creative Commons Attribution-NonCommercial 3.0 Unported Licence.

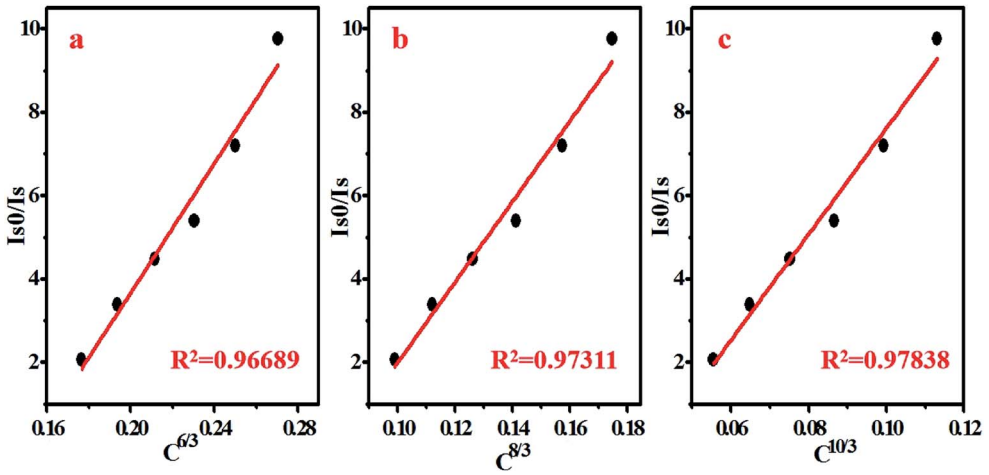


Fig. 11 Dependence of $I_{s0}/I_s$ of $Ce^{3+}$ and $Tb^{3+}$ on $C^{6/3}$, $C^{8/3}$ and $C^{10/3}$ in BYP:0.4$Tb^{3+}$,y$Mn^{2+}$y$Mn^{2+}$.

can be calculated by expression (4), for BYP:0.4$Tb^{3+}$,y$Mn^{2+}$, $\chi_c$ is calculated to be 0.42 and the $Rc_{Tb-Mn}$ is calculated to be 13.84 Å which is obviously larger than the maximum distance of 5 Å for the exchange interaction. Thus it can be confirmed that the type of interaction between $Tb^{3+}$ and $Mn^{2+}$ is multipolar interaction. The linear relationship between $I_0/I$ and $C^{n/3}$ for BYP:0.4$Tb^{3+}$,y$Mn^{2+}$ are illustrated in Fig. 11a, and a well fitted curve can be gotten when $n = 10$ and $R^2 = 0.97838$, therefore, it can be confirmed that the $ET_{Tb-Mn}$ mechanism is quadrupole–quadrupole interaction.

The Commission Internationale de L'Eclairage (CIE) chromaticity coordinates of BYP:0.4$Tb^{3+}$,y$Mn^{2+}$ ($y = 0.02$–0.12) was calculated basing on the relevant emission spectra under 377 nm excitation. The calculated results along with luminescent photographs of related phosphors are depicted in Fig. 12, the emission color of BYP:0.4$Tb^{3+}$,y$Mn^{2+}$ can be modulated from yellow-greenish (0.3329, 0.5275) to white (0.3936, 0.3562). Thus, BYP:0.4$Tb^{3+}$,y$Mn^{2+}$ can act as a color-tunable material which can be used in near UV based white LEDs.

The temperature-dependent emission spectra of BYP:0.4$Tb^{3+}$,0.12$Mn^{2+}$ excited by 377 nm was measured and shown in Fig. 13a, and the emission intensity of $Tb^{3+}$ and $Mn^{2+}$ is presented in Fig. 13b. It can be seen from Fig. 13a that the emission peak of $Mn^{2+}$ shifts from 600 nm to 588 nm due to the thermally active phonon-assisted excitation from lower energy levels to higher energy levels in the excited state of $Mn^{2+}$.[24] Because of the thermal quenching, the emission intensity of $Mn^{2+}$ decreases continually with the increase of temperature and remains 80.5% of the initial value (300 K) when the temperature reaches 425 K. However, the emission intensity of $Tb^{3+}$ increases continually, and when the temperature reaches 425 K the emission intensity rises to 111.6% of the initial value.

The abnormal change of emission intensity of $Tb^{3+}$ is also caused by the defects in BYP:0.4$Tb^{3+}$,0.12$Mn^{2+}$. Fig. 14a depicts the thermoluminescence spectrum of BYP:0.4$Tb^{3+}$,0.12$Mn^{2+}$, as

| CIE chromaticity coordinates of BYP:0.4$Tb^{3+}$,y$Mn^{2+}$ | |
|---|---|
| y=0.02 | (0.3329 , 0.5275) |
| y=0.04 | (0.3518 , 0.4715) |
| y=0.06 | (0.3700,0.4498) |
| y=0.08 | (0.3747 , 0.4272) |
| y=0.10 | (0.3944 , 0.3700) |
| y=0.12 | (0.3936 , 0.3562) |

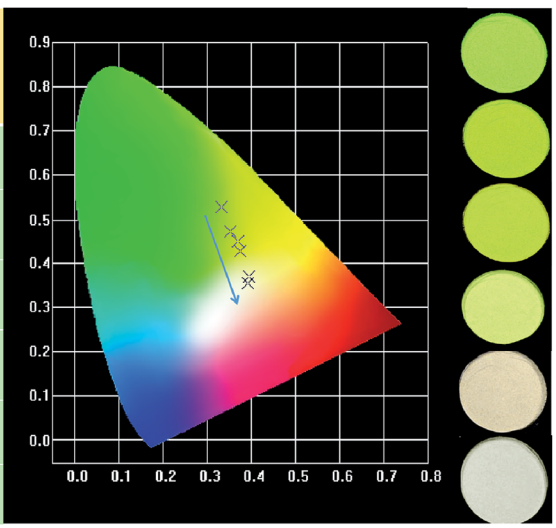

Fig. 12 CIE chromaticity coordinates of BYP:0.4$Tb^{3+}$,y$Mn^{2+}$ ($y = 0.02$–0.12) along with their luminescent photographs.

Open Access Article. Published on 25 September 2019. Downloaded on 6/30/2024 12:57:32 PM.
This article is licensed under a Creative Commons Attribution-NonCommercial 3.0 Unported Licence.

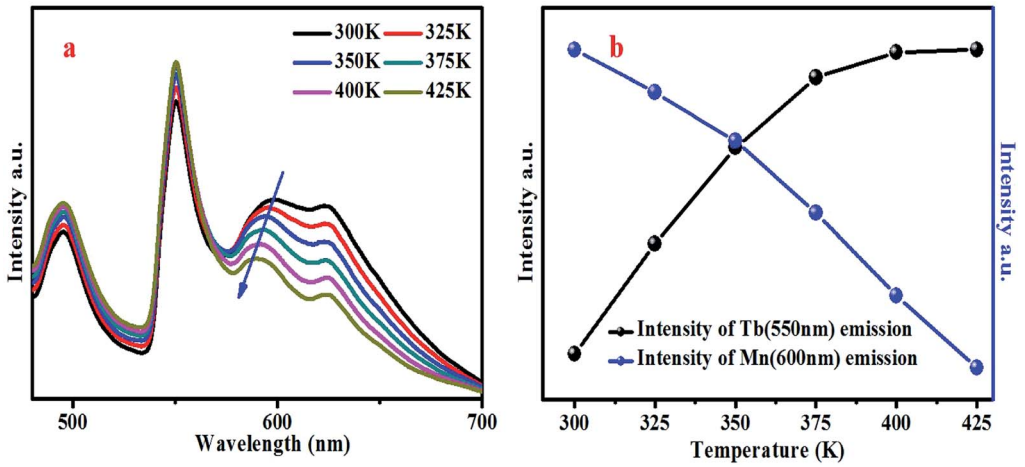


Fig. 13 (a) Temperature-dependent emission spectra of BYP:0.4$Tb^{3+}$,0.12$Mn^{2+}$ excited by 377 nm. (b) Relative intensity of $Tb^{3+}$ and $Mn^{2+}$ in the temperature-dependent emission spectra.

mentioned in Chapter 3.2: the emission intensity change of $Ce^{3+}$ and $Tb^{3+}$ in temperature-dependent emission spectra of BYP:0.05$Ce^{3+}$,0.45$Tb^{3+}$. Fig. 14b is the schematic diagram on how the defects affect the emission intensity of $Tb^{3+}$ in BYP:0.4$Tb^{3+}$,0.12$Mn^{2+}$.

### 3.4 Luminescence and energy transfer of BYP:z$Ce^{3+}$,0.4$Tb^{3+}$,0.12$Mn^{2+}$

Fig. 15a shows the emission spectra of BYP:0.15$Ce^{3+}$,0.4$Tb^{3+}$,0.12$Mn^{2+}$ excited by 330 nm, it can be seen that the emission peaks of $Ce^{3+}$ (390 nm), $Tb^{3+}$ (550 nm) and $Mn^{2+}$ (600 nm) coexist in the emission spectra covering blue, yellow, green and red region, thus, the efficient white emission is expectable. Fig. 15b depicts the excitation spectra of BYP:0.15$Ce^{3+}$,0.4$Tb^{3+}$,0.12$Mn^{2+}$ monitored at 390 nm, 550 nm and 600 nm, from which one can see that the obtained three spectra have the similar profile, it means that there is energy transfer among $Ce^{3+}$, $Tb^{3+}$ and $Mn^{2+}$. To further investigate the luminescence and energy transfer, the emission spectra of BYP:z$Ce^{3+}$,0.4$Tb^{3+}$,0.12$Mn^{2+}$ under 330 nm excitation are shown in Fig. 15c, the relative intensity of $Ce^{3+}$, $Tb^{3+}$ and $Mn^{2+}$ is depicted in Fig. 15d. It can be seen that the emission intensity of $Ce^{3+}$, $Tb^{3+}$ and $Mn^{2+}$ increase continuously with increasing $Ce^{3+}$ concentration, it indicates that there are $ET_{Ce-Tb}$, $ET_{Ce-Mn}$ and $ET_{Tb-Mn}$ in BYP:z$Ce^{3+}$,0.4$Tb^{3+}$,0.12$Mn^{2+}$.

Fig. 16 shows the Commission Internationale de L'Eclairage (CIE) chromaticity coordinates of BYP:z$Ce^{3+}$,0.4$Tb^{3+}$,0.12$Mn^{2+}$ ($z$ = 0.01–0.11) and luminescent photographs of related phosphors when excited by 330 nm UV excitation. The emission color of BYP:z$Ce^{3+}$,0.4$Tb^{3+}$,0.12$Mn^{2+}$ can be modulated from white (0.3030 , 0.2893) with high color temperature to white (0.4096 , 0.3770) with low color temperature, *viz.*, a series of single-phased white light-emitting phosphors are realized successfully, and it maybe a potential application in white LEDs.

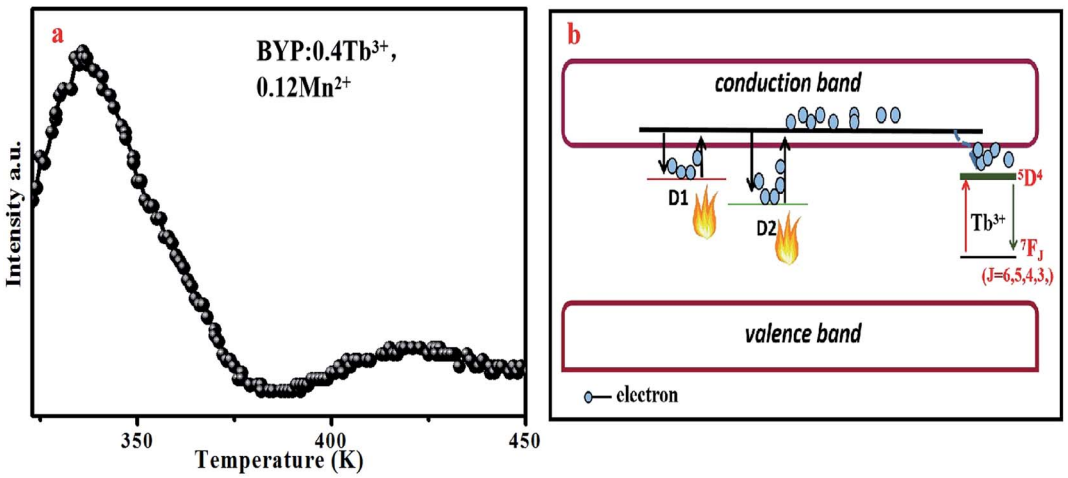


Fig. 14 (a) Thermoluminescence spectrum of BYP:0.4$Tb^{3+}$,0.12$Mn^{2+}$. (b) Schematic diagram of the interaction between the defect and temperature-dependent emission intensity in BYP:0.4$Tb^{3+}$,0.12$Mn^{2+}$.


This journal is © The Royal Society of Chemistry 2019

Open Access Article. Published on 25 September 2019. Downloaded on 6/30/2024 12:57:32 PM.
This article is licensed under a Creative Commons Attribution-NonCommercial 3.0 Unported Licence.

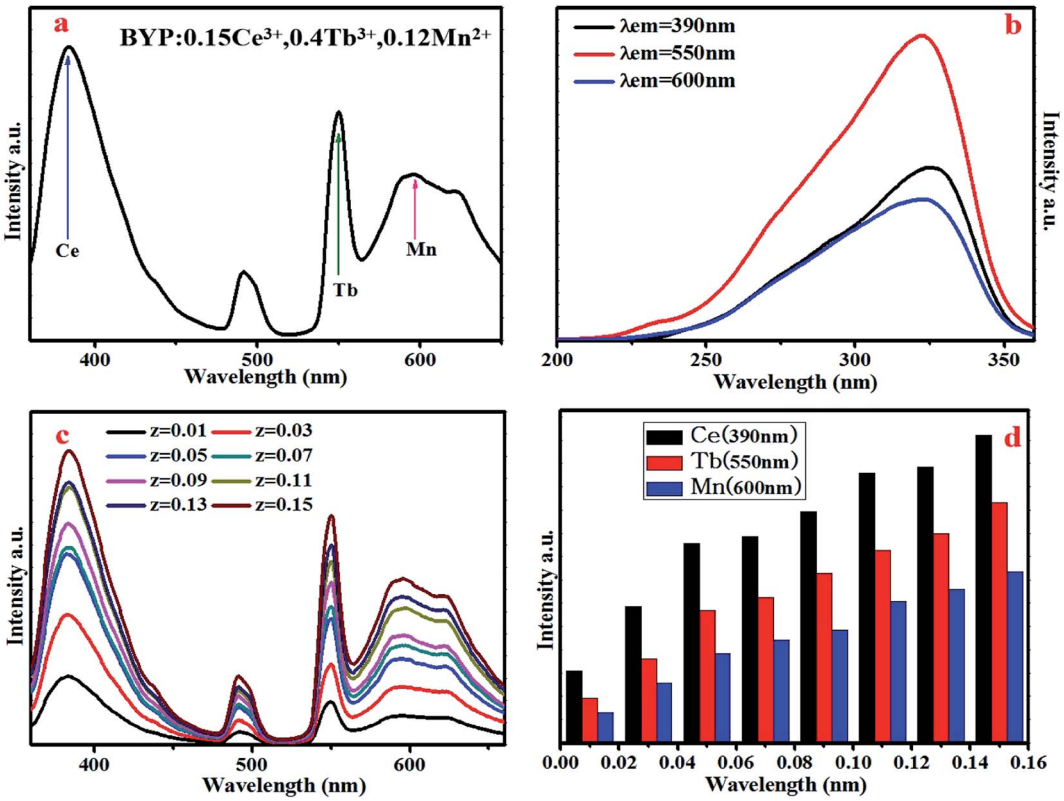


Fig. 15 (a) Emission spectrum of BYP:0.15$Ce^{3+}$,0.4$Tb^{3+}$,0.12$Mn^{2+}$ ($\lambda_{ex}$ = 330 nm). (b) Excitation spectra of BYP:0.15$Ce^{3+}$,0.4$Tb^{3+}$,0.12$Mn^{2+}$ ($\lambda_{em}$ = 390 nm, 550 nm and 600 nm). (c) Emission spectra of BYP:z$Ce^{3+}$,0.4$Tb^{3+}$,0.12$Mn^{2+}$ ($\lambda_{ex}$ = 330 nm). (d) Relative intensity of $Ce^{3+}$, $Tb^{3+}$ and $Mn^{2+}$ in BYP:z$Ce^{3+}$,0.4$Tb^{3+}$,0.12$Mn^{2+}$.

As a representative, BYP:0.03$Ce^{3+}$,0.4$Tb^{3+}$,0.12$Mn^{2+}$ was chosen to explore the thermal stabilities. Fig. 17a depicts the temperature-dependent emission spectra of BYP:0.03$Ce^{3+}$,0.4$Tb^{3+}$,0.12$Mn^{2+}$ under 330 nm UV excitation, Fig. 17b shows the emission intensity of $Ce^{3+}$, $Tb^{3+}$ and $Mn^{2+}$. The emission peak of $Mn^{2+}$ shifts from 600 nm to 587 nm with increasing the temperature and the reason is the same as that mentioned above, it is because of the thermally active phonon-assisted of $Mn^{2+}$. With rising of temperature, the emission intensity of $Mn^{2+}$ decreases due to thermal quenching effect

| CIE chromaticity coordinates of BYP: z$Ce^{3+}$, 0.4$Tb^{3+}$,0.12$Mn^{2+}$ | |
|---|---|
| z=0.01 | (0.3030 , 0.2893) |
| z=0.03 | (0.3308 , 0.3083) |
| z=0.05 | (0.3408, 0.3233) |
| z=0.07 | (0.3651 , 0.3431) |
| z=0.09 | (0.3837 , 0.3574) |
| z=0.11 | (0.4096 , 0.3770) |

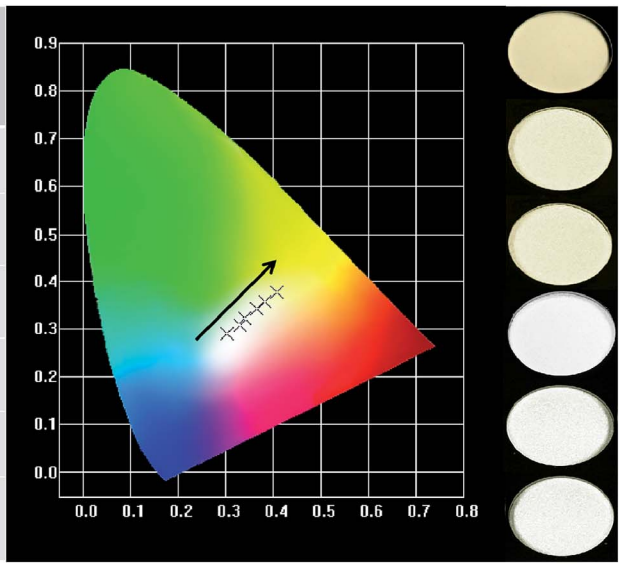


Fig. 16 CIE chromaticity coordinates of BYP:z$Ce^{3+}$,0.4$Tb^{3+}$,0.12$Mn^{2+}$ (z = 0.01–0.11) along with their luminescent photographs.

Open Access Article. Published on 25 September 2019. Downloaded on 6/30/2024 12:57:32 PM.
This article is licensed under a Creative Commons Attribution-NonCommercial 3.0 Unported Licence.

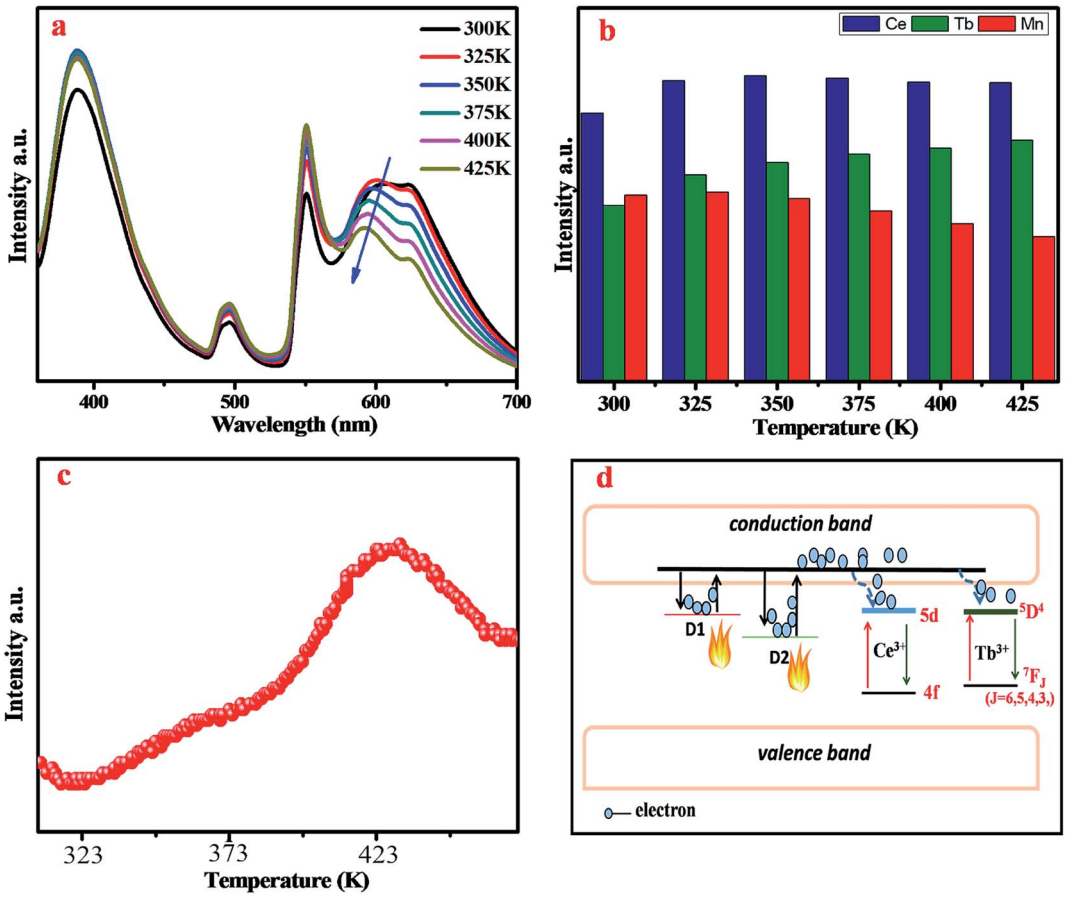


Fig. 17 (a) Temperature-dependent emission spectra of BYP:0.4$Tb^{3+}$,0.12$Mn^{2+}$ under 330 nm UV excitation. (b) Relative intensity of $Ce^{3+}$, $Tb^{3+}$ and $Mn^{2+}$. (c) Thermoluminescence spectrum of BYP:0.03$Ce^{3+}$,0.4$Tb^{3+}$,0.12$Mn^{2+}$. (d) Schematic diagram of the interaction between the defect and temperature-dependent emission intensity in BYP:0.03$Ce^{3+}$,0.4$Tb^{3+}$,0.12$Mn^{2+}$.

and it still remains 80.8% of the initial value when the temperature rises to 425 K. The emission intensity of $Ce^{3+}$ shows a first increase and then decrease, the emission intensity of $Tb^{3+}$ increases constantly with increasing temperature. Fig. 17c presents the thermoluminescence spectrum of BYP:0.03$Ce^{3+}$,0.4$Tb^{3+}$,0.12$Mn^{2+}$. The change in emission intensity of $Ce^{3+}$ and $Tb^{3+}$ is ascribed to the same theory as mentioned in chapter 3.2: the emission intensity change of $Ce^{3+}$ and $Tb^{3+}$ in temperature-dependent emission spectra of BYP:0.05$Ce^{3+}$,0.45$Tb^{3+}$. Fig. 17d is the schematic diagram on how the defects affect the emission intensity of $Ce^{3+}$ and $Tb^{3+}$ in BYP:0.03$Ce^{3+}$,0.4$Tb^{3+}$,0.12$Mn^{2+}$.

## 4 Conclusions

In summary, a series of eulytite-typed and single-phased phosphors BYP:0.05$Ce^{3+}$, $x$$Tb^{3+}$, BYP:0.05$Ce^{3+}$, $y$$Mn^{2+}$ and BYP:$z$$Ce^{3+}$,0.3$Tb^{3+}$,0.14$Mn^{2+}$ were synthesized successfully. The energy transfer from $Ce^{3+}$ to $Tb^{3+}$ and $Tb^{3+}$ to $Mn^{2+}$ were confirmed by analyzing its spectra and fluorescence lifetime. The thermal stability of samples is extraordinary, and it had been proved that the unusual temperature performance is caused by the defects in the samples. Finally, a series of single-phased color-tunable with high thermal stability phosphors were obtained, especially BYP:$z$$Ce^{3+}$,0.3$Tb^{3+}$,0.14$Mn^{2+}$, it can emit warm white light and the color temperature can be modulated by the energy among $Ce^{3+}$, $Tb^{3+}$ and $Mn^{2+}$. Thus, it may have application potential in white LEDs.

## Conflicts of interest

There are no conflicts to declare.

## Acknowledgements

The work is supported by the National Natural Science Foundation of China (Nos. 51672066, 51902080), the Funds for Distinguished Young Scientists of Hebei Province, China (No. A2018201101), and the Natural Science Foundation of Hebei Province, China (No. E2019201223).

## References

1 J. W. Qiao, Z. Zhao, Q. L. Liu and Z. G. Xia, Recent advances in solid-state LED phosphors with thermally stable luminescence, *J. Rare Earths*, 2019, **37**, 565–572.


This journal is © The Royal Society of Chemistry 2019

Open Access Article. Published on 25 September 2019. Downloaded on 6/30/2024 12:57:32 PM.
This article is licensed under a Creative Commons Attribution-NonCommercial 3.0 Unported Licence.

2 C. Li, H. W. Zheng, H. W. Wei, S. J. Qiu, L. Xu, X. M. Wang and H. Jiao, Color tunable and white light emitting $Ca_2Si_5N_8$:$Ce^{3+}$, $Eu^{2+}$ phosphor via efficient energy transfer for near-UV white LEDs, *Dalton Trans.*, 2018, **47**(19), 6860–6867.

3 F. B. Xiong, S. X. Liu, H. F. Lin, X. G. Meng, S. Y. Lian and W. Z. Zhu, A novel white-light-emission phosphor $Dy^{3+}$-doped $CaLaB_7O_{13}$ under UV excitation, *Opt. Laser Technol.*, 2018, **106**, 29–33.

4 M. Zhao, H. Liao, M. S. Molokeev, Y. Zhou, Q. Zhang, Q. Liu and Z. Xia, Emerging ultra-narrow-band cyan-emitting phosphor for white LEDs with enhanced color rendition, *Light: Sci. Appl.*, 2019, **8**, 38.

5 X. Y. Huang and H. Guo, $LiCa_3MgV_3O_{12}$:$Sm^{3+}$: A new high-efficiency white-emitting phosphor, *Ceram. Int.*, 2018, **44**, 10340–10344.

6 N. T. K. Chi, N. T. Tuan, N. T. K. Lien and H. Nguyen, Red Emission of $SrAl_2O_4$:$Mn^{4+}$ Phosphor for Warm White Light-Emitting Diodes, *J. Electron. Mater.*, 2018, (10), 1–8.

7 J. X. Hu, T. H. Huang, Y. P. Zhang, B. Lu, H. Q. Ye, B. J. Chen, H. P. Xia and C. Y. Ji, Enhanced deep-red emission from $Mn^{4+}$/$Mg^{2+}$ co-doped $CaGdAlO_4$ phosphors for plant cultivation, *Dalton Trans.*, 2019, **48**, 2455–2466.

8 J. T. Zhao, X. Y. Sun and Z. Q. Wang, $Ce^{3+}$/$Eu^{2+}$ doped $SrSc_2O_4$ phosphors: Synthesis, luminescence and energy transfer from $Ce^{3+}$ to $Eu^{2+}$, *Chem. Phys. Lett.*, 2018, **691**, 68–72.

9 Z. Y. Mao, J. J. Chen, J. Li and D. J. Wang, Dual-responsive $Sr_2SiO_4$:$Eu^{2+}$-$Ba_3MgSi_2O_8$:$Eu^{2+}$,$Mn^{2+}$ composite phosphor to human eyes and plant chlorophylls applications for general lighting and plant lighting, *Chem. Eng. J.*, 2016, **284**, 1003–1007.

10 S. Wang, Y. F. Li, L. G. Feng, L. Z. Zhang, Y. Zhang, X. L. Su, W. Ding and F. Yun, Laser patterning of $Y_3Al_5O_{12}$:$Ce^{3+}$ ceramic phosphor platelets for enhanced forward light extraction and angular color uniformity of white LEDs, *Opt. Express*, 2016, **24**(15), 17522–17531.

11 Y. Zhang, X. J. Zhang, H. R. Zhang, L. L. Zheng, Y. Zeng, Y. Lin, Y. L. Liu and B. F. Lei, Tunable emission from green to red in the $GdSr_2AlO_5$:$Tb^{3+}$,$Eu^{3+}$phosphor via efficient energy transfer, *RSC Adv.*, 2018, **8**(7), 3530–3535.

12 T. Senden, E. J. V. Harten and A. Meijerink, Synthesis and narrow red luminescence of $Cs_2HfF_6$:$Mn^{4+}$ a new phosphor for warm white LEDs, *J. Lumin.*, 2018, **194**, 131–138.

13 H. P. You, Y. H. Song, G. Jia and G. Y. Hong, Energy transfer from $Tb^{3+}$ to $Mn^{2+}$ in $LaMgAl_{11}O_{19}$:Tb, Mn phosphors, *Opt. Mater.*, 2008, **31**(2), 342–345.

14 Z. M. Zhao, Z. G. Xia, X. X. Huang, L. X. Ning, G. Romain, M. S. Molokeev, Y. Y. Zhou, Y. C. Chuang, Q. Y. Zhang, Q. L. Liu and K. R. Poeppelmeier, Li substituent tuning of LED phosphors with enhanced efficiency, tunable photoluminescence, and improved thermal stability, *Sci. Adv.*, 2019, **5**, eaav0363.

15 J. R. Sun, P. Huang, Y. F. Liu, L. Wang, C. E. Cui, Q. F. Shi and Y. Tian, Color-tunable $Ca_{10}Na(PO_4)_7$:$Ce^{3+}$/$Tb^{3+}$/$Mn^{2+}$, phosphor via energy transfer, *J. Rare Earths*, 2018, **36**(6), 567–574.

16 W. Lü, H. W. Xu, M. M. Hao, H. C. Wang and X. J. Kang, Tunable full-color emitting $Na_2Ba_6(Si_2O_7)(SiO_4)_2$:$Ce^{3+}$, $Eu^{2+}$, $Tb^{3+}$, $Mn^{2+}$, phosphor for UV white LEDs: Photoluminescence and energy transfer, *J. Alloys Compd.*, 2018, **752**, 231–237.

17 Y. Chen, Z. J. Wang, W. G. Ding, X. Li, Q. Bao, J. J. Liu, K. L. Qiu, X. Y. Meng, Z. P. Yang and P. L. Li, A single-phase white light emitting phosphor $Ba_3Y(PO_4)_3$:$Ce^{3+}$/$Eu^{2+}$/$Mn^{2+}$: Luminescence, energy transfer and thermal stability, *J. Lumin.*, 2019, **210**, 322–334.

18 C. H. Huang, T. W. Kuo and T. M. Chen, Thermally stable green $Ba_3Y(PO_4)_3$:$Ce^{3+}$,$Tb^{3+}$ and red $Ca_3YAlO_3(BO_3)_4$:$Eu^{3+}$ phosphors for white-light fluorescent lamps, *Opt. Express*, 2011, **19**(S1), A1–A6.

19 N. Guo, C. Z. Jia, J. Li, Y. F. Zhao, R. Z. Oyang and W. Lü, Color Tuning and Energy Transfer in $Eu^{2+}$/$Mn^{2+}$-Doped $Ba_3Y(PO_4)_3$ Eulytite-Type Orthophosphate Phosphors, *RSC Adv.*, 2015, **5**(58), 46517–46524.

20 Y. B. Chen, K. W. Cheah and M. L. Gong, Low thermal quenching and high-efficiency $Ce^{3+}$, $Tb^{3+}$-co-doped $Ca_3Sc_2Si_3O_{12}$ green phosphor for white light-emitting diodes, *J. Lumin.*, 2011, **131**(8), 1589–1593.

21 C. Wang, P. L. Li, Z. J. Wang, Z. P. Yang, Z. L. Li, M. M. Tian, J. G. Cheng and Y. S. Sun, Crystal structure, luminescence properties, energy transfer and thermal properties of a novel color-tunable, white light-emitting phosphor $Ca_{9-x-y}Ce(PO_4)_7$:$xEu^{2+}$,$yMn^{2+}$, *Phys. Chem. Chem. Phys.*, 2016, **18**(41), 28661–28673.

22 S. C. Xu, Z. J. Wang, P. L. Li, T. Li, Q. Y. Bai, J. Sun and Z. P. Yang, White-emitting phosphor $Ba_2B_2O_5$:$Ce^{3+}$, $Tb^{3+}$, $Sm^{3+}$: luminescence, energy transfer, and thermal stability, *J. Am. Ceram. Soc.*, 2017, **100**, 2069–2080.

23 X. Li, P. L. Li, Z. J. Wang, S. M. Liu, Q. Bao, X. Y. Meng and K. L. Qiu, Color-tunable luminescence properties of $Bi^{3+}$ in $Ca_5(BO_3)_3F$ via changing site occupation and energy transfer, *Chem. Mater.*, 2017, **29**(20), 8792–8803.

24 X. G. Zhang, J. G. Xu and M. L. Gong, Site-occupancy, luminescent properties and energy transfer of a violet-to-red color-tunable phosphor $Ca_{10}Li(PO_4)_7$:$Ce^{3+}$, $Mn^{2+}$, *J. Lumin.*, 2017, **183**, 348–354.

25 Y. Zhang, X. J. Zhang, H. R. Zhang, L. L. Zheng, Y. Zeng, Y. Lin, Y. L. Liu and B. F. Lei, Tunable emission from green to red in the $GdSr_2AlO_5$:$Tb^{3+}$, $Eu^{3+}$ phosphor via efficient energy transfer, *RSC Adv.*, 2018, **8**, 3530–3535.

26 G. G. Li, Y. Tian, Y. Zhao and J. Lin, Recent progress in luminescence tuning of $Ce^{3+}$ and $Eu^{2+}$-activated phosphors for pc-WLEDs, *Chem. Soc. Rev.*, 2016, **47**(1), 8688–8713.

27 F. Xiao, R. X. Yi, H. L. Yuan, G. J. Zang and C. N. Xie, Color tunable emission and energy transfer of $Ce^{3+}$/$Dy^{3+}$ codoped $Ba_3La_2(BO_3)_4$ phosphor for UV white LEDs, *Spectrochim. Acta, Part A*, 2018, **202**, 352–358.

28 H. J. Guo, Y. T. Wang, G. Li, J. Liu, P. Feng and D. W. Liu, Cyan emissive super-persistent luminescence and thermoluminescence in $BaZrSi_3O_9$:$Eu^{2+}$, $Pr^{3+}$ phosphors, *J. Mater. Chem. C*, 2017, **5**(11), 2844–2851.

Open Access Article. Published on 25 September 2019. Downloaded on 6/30/2024 12:57:32 PM.
This article is licensed under a Creative Commons Attribution-NonCommercial 3.0 Unported Licence.

29 Z. L. Li, Z. J. Wang, P. L. Li, J. G. Cheng, M. M. Tian, C. Wang and Z. P. Yang, Improvement of thermally stable and photoluminescence in $Sr_{0.8}Ca_{0.2}Al_2Si_2O_8:Eu^{2+}$ by the substitution of Si-Na # Al-Sr and Ca # Sr on structural modifications, *Dalton Trans.*, 2017, **41**, 14310–14317.

30 Q. Y. Bai, Z. J. Wang, P. L. Li, S. C. Xu, T. Li, J. G. Cheng and Z. P. Yang, Utilizing $Tb^{3+}$ as the energy transfer bridge to connect $Eu^{3+}$-Zn2GeO4 host: Realization of efficient $Eu^{3+}$ red emission, *Mater. Des.*, 2016, **108**, 597–607.


This journal is © The Royal Society of Chemistry 2019